SSRG International Journal of Mechanical Engineering
ISSN: 2348-8360/ https://doi.org/10.14445/23488360/IJME-V13I7P114

Volume 13 Issue 7, 164-173, July 2026

Original Article

Mechanistic Evaluation of Nano-Additive-Contaminant Interactions in Lubricated Rolling Bearings: Tribofilm Evolution and Wear Behavior

R. T. Chander[1*], P S. Chakraborty[2], S. Nallusamy[3], V. S. Hariharan[4]

[1,2,3]*School of Engineering Management and Continuing Education, Jadavpur University, Kolkata, India.*
[4]*Department of Mechanical Engineering, Balaji Institute of Technology and Science, Warangal, Telangana, India.*

[1*]*Corresponding Author : rtchander6@gmail.com*

Received: 12 April 2026 Revised: 14 June 2026 Accepted: 10 July 2026 Published: 30 July 2026

Abstract *- The present study investigates the synergistic and antagonistic effects of engineered nanoparticle additives and hard solid contaminants in lubricated rolling bearings. For a comprehensive experimental assessment, three nanoparticle additives, such as Tungsten Disulfide (WS_2), Graphene Nanoplatelets (GNP) and Alumina (Al_2O_3), were dispersed in a base mineral oil to study their influence on the friction, wear and tribochemical behaviour of bearings under quartz particulate contamination. The analysis was done through controlled experiments in a custom-made bearing test rig at multiple loads and speeds with continuous monitoring of friction torque, temperature and vibration. Also, to characterize wear morphologies and tribofilm composition, post-test analyses were carried out using Scanning Electron Microscopy (SEM), Energy-Dispersive X-ray Spectroscopy (EDS), X-ray Photoelectron Spectroscopy (XPS), and Raman spectroscopy. From the analysis, results revealed that WS_2 and GNP nanoparticles showed synergistic effects, forming protective tribofilms that significantly reduced wear, surface roughness, and vibration amplitude. In contrast, Al_2O_3 nanoparticles revealed antagonistic behaviour, promoting abrasive wear due to agglomeration and amplified third-body interactions. The collective analysis of mechanical and surface data expounds the underlying mechanisms of film formation, particle entrapment, and surface repair. Besides, this study provides new insights into the selection and formulation of nano-additives for lubricants intended for contaminated environments, contributing to extended bearing life and improved operational reliability.*

Keywords - *Nanoparticle additives, Solid contamination, Tribofilm, Rolling bearings, Wear Mechanism, Vibration analysis.*

1. Introduction

Rolling element bearings are regarded as critical components in rotating machinery, providing low-friction motion and supporting dynamic loads during continuous operation. Actually, their performance and lifetime are strongly influenced by the quality of lubrication selected. In real industrial environments, lubricant oil is often subjected to solid particulate contamination arising from wear debris, seal degradation, or ingress of external dust particles [1, 2]. These contaminants can disrupt the Elasto-Hydrodynamic Lubrication (EHL) film, promote three-body abrasion, and accelerate surface fatigue, thereby contributing to early bearing failure [3]. Moreover, recent studies have shown that even a minor concentration of hard particles such as silica or alumina can significantly increase vibration amplitude and wear rate in rolling contacts [4].

To overcome this, substantial research has been devoted to understanding the tribological effects of solid contaminants in lubricated systems. Nevertheless, early investigations primarily focused on the influence of particle size, hardness, and concentration on wear and friction. For instance, fine particles smaller than the oil film thickness were found to embed into surface asperities and eventually act as polishing agents, while larger particles tend to abrade surfaces and initiate fatigue cracks [5]. More recently, studies, including those done by Suresh et al. and other researchers, have shown that contamination changes not only the frictional characteristics but also the vibration and acoustic emission signatures of bearings, thereby offering a potential pathway for condition monitoring [6].

Solid-particle contamination and nano-additive lubrication have generally been investigated as separate tribological problems [7]. Studies on contaminated bearings have shown that hard particles disrupt lubricant-film continuity, promote three-body abrasion, and alter friction, temperature, vibration, and surface-damage behaviour [8]. In contrast, nano-additive studies commonly evaluate WS_2, graphene-based materials, or metal-oxide nanoparticles in clean oils or simplified sliding contacts. Their reported benefits are mainly associated with lamellar shear, transfer-film formation, surface filling, and mending effects. Recent studies on contaminated rolling bearings have focused mainly on contaminant capture, surface modification, and dynamic monitoring, whereas studies on nanolubricants have focused mainly on dispersion stability, friction reduction, and tribofilm formation [9].

However, limited information is available on the simultaneous interaction between engineered nano-additives and hard contaminant particles in a lubricated rolling bearing. In particular, it remains unclear whether an additive that performs well in clean oil can retain its protective function when quartz particles enter the rolling contact. It is also unclear how additive hardness, morphology, and film-forming ability determine whether the additive–contaminant interaction becomes protective or abrasive [10].

Previous research can be grouped into three main areas. The first area concerns contaminant-induced bearing damage, where particle size, hardness, concentration, and morphology have been linked to ploughing, indentation, fatigue initiation, and increased vibration. The second area concerns nano-additive lubrication, where WS_2 and graphene-based particles have been reported to form low-shear surface films, while the behaviour of hard oxide nanoparticles has been found to depend strongly on concentration and dispersion stability. The third area concerns tribofilm characterization through SEM, EDS, XPS, and Raman spectroscopy. Although these studies provide valuable individual findings, few have combined controlled rolling-bearing tests, hard quartz contamination, chemically different nano-additives, vibration monitoring, and surface-chemical analysis within the same experimental design [11-14]. The novelty of the present study lies in the controlled comparison of three chemically and mechanically different nano-additives, namely lamellar WS_2, sheet-like graphene nanoplatelets, and hard ceramic Al_2O_3, under identical quartz-contaminated rolling-bearing conditions. Unlike studies based only on friction or wear measurements, the present investigation combines friction torque, housing temperature, vibration, specific wear rate, SEM/EDS, XPS, and Raman spectroscopy. This combined mechanical, dynamic, and tribochemical approach is used to distinguish protective tribofilm formation from agglomeration-driven third-body abrasion.

Accordingly, the objectives of the study are to: (i) quantify the effects of additive type and concentration on the friction, temperature, vibration, and wear behaviour of contaminated rolling bearings at different loads and speeds; (ii) identify the morphology and chemical composition of the additive-derived surface films; and (iii) explain why WS_2 and GNP retain protective behaviour while Al_2O_3 produces an adverse interaction with quartz particles. The findings provide a mechanistic basis for selecting nano-additives for rolling bearings operating in particle-contaminated environments.

2. Materials and Methods

2.1. Materials and Lubricant Preparation

The base lubricant extensively used in this study was a mineral-based ISO VG 32 oil with a kinematic viscosity of 32 cSt at 40°C and a density of 870 kg. m^{-3}. This grade of oil is normally applied in rolling bearings because of its good oxidative stability. The solid contaminant employed was quartz sand (SiO_2) with a particulate size in the range of 20–50 μm and hardness around 7 Mohs, similar to previous contamination studies. Prior to use, the particles were ultrasonically cleaned in acetone and oven-dried before use to remove residual moisture. Three engineered nanoparticle additives were selected to represent distinct classes of lubricant modifiers:

- Tungsten disulfide (WS_2) – layered dichalcogenide solid lubricant with very low shear strength;
- Graphene nanoplatelets (GNP) – carbon-based additive capable of forming low-shear protective films; and
- Alumina (Al_2O_3) – a hard ceramic oxide nanoparticle representative of abrasive behavior.

Table 1. Physical and chemical characteristics of materials used

Material	Type / Composition	Average size	Density (g.cm^{-3})	Hardness	Function
Quartz (SiO_2)	Angular solid particles	20–50 μm	2.65	7 (Mohs)	Contaminant
WS_2 nanoparticles	Lamellar solid lubricant	60 nm	7.5	1–1.5 (Mohs)	Nano-additive
Graphene nanoplatelets (GNP)	Carbon-based sheets	50 nm (thickness < 10 nm)	2.2	–	Nano-additive
Al_2O_3 nanoparticles	Ceramic oxide	70 nm	3.9	9 (Mohs)	Nano-additive

All nanoparticles (purity > 99%, 40–80 nm, Sigma-Aldrich USA) were dispersed in the base oil at 0 wt % (control), 0.05 wt %, and 0.2 wt % concentrations as shown in Table 2. Nanoparticle concentrations of 0.05 and 0.20 wt% were selected to represent a low-dose and a higher-dose condition while remaining within the concentration range commonly examined for nanolubricants. The 0.05 wt% level was used to assess film-forming performance at limited particle loading, whereas the 0.20 wt% level was used to examine whether increased particle availability improved surface protection or promoted concentration-dependent agglomeration.

Quartz particles were added at a concentration of 0.05 wt%, equivalent to approximately 435 mg/L, relative to the mass of the lubricant. This concentration was selected based on previously reported ball-bearing experiments using ISO VG 32 mineral oil, in which quartz contamination levels ranging from 0.04 to 0.71 g/L produced measurable changes in vibration and contaminant-induced wear. The selected concentration is close to the previously examined intermediate level of 0.44 g/L and was therefore adopted to produce measurable abrasive interaction during the five-hour test while avoiding an excessively severe contamination condition that could cause rapid bearing failure.Homogeneous dispersions were prepared using an ultrasonic probe (20 kHz, 200 W) for 30 min at room temperature with 0.1 wt % oleic acid as a dispersant.

The WS_2, GNP, and Al_2O_3 nanoparticles were commercially procured in pre-characterized form, and the supplier-certified specifications regarding particle size and crystallinity were adopted for the present investigation. Quartz contaminants were mixed into the oil immediately before each test by magnetic stirring for 10 min [14].

2.2. Experimental Setup

All the experiments were conducted on a custom bearing test rig designed to apply controlled load, speed, and lubrication conditions. A deep-groove ball bearing (type 6204, SKF), mounted on a shaft driven by a variable speed motor as shown in Figure 1, was used for the rig. As in previous tribology studies [15], radial loads were applied that ranged from 500 N to 2000 N using a mechanical lever arrangement.

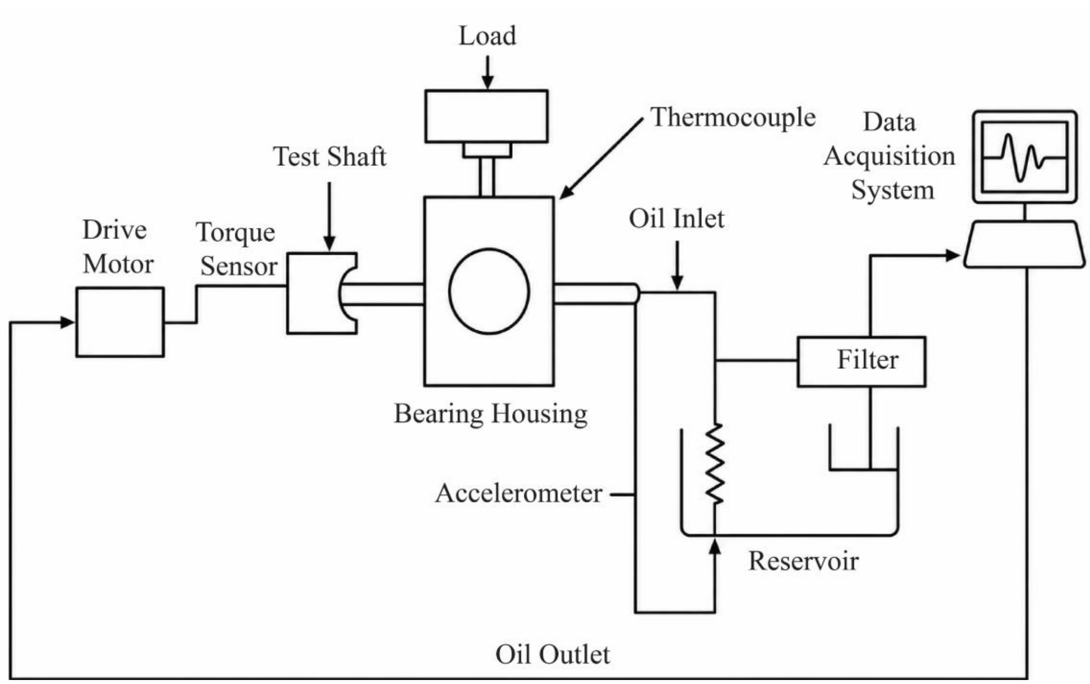

Fig. 1 Schematic of the experimental bearing test rig used for evaluating nanoparticle contaminant interactions under lubricated conditions

The lubricant was circulated through the oil supply system (100 mL.min^{-1}) with a thermostatic controller maintained at 40±2°C. The bearing housing was equipped with a K-type thermocouple for temperature monitoring, a piezoelectric accelerometer for vibration monitoring and a torque transducer to measure friction. Through LabVIEW, a data-acquisition system (NI USB-4432, 102.4 kHz) has been used to collect vibration and torque signals. After that, MATLAB [16] was used to post-process the data.

2.3. Experimental Procedure

Before testing, all components underwent ultrasonic cleaning in acetone and drying. The bearing housing received approximately 50 mL of the prepared lubricant mix. Each run lasted for 5 h or until a sustained increased vibration amplitude (> 30%) indicated advanced wear. The operating conditions consisted of three speeds and two loads. The speeds were 1000, 2000 and 3000 rpm. The loads were 1000 N and 2000 N. Tests were performed under controlled quartz contamination at the specified nanoparticle concentrations, and each condition was repeated three times. In addition, tests were carried out on a custom-built rolling bearing test rig that operated under controlled conditions of load, speed, temperature and lubrication. Though not specifically addressed by a single ASTM standard, the experimental operations, wear-rate calculations, and tribological interpretations of contaminated rolling bearing tests were performed in accordance with the generalities of the standards ASTM G99 and ASTM G133 for tribological testing. The measurements of acoustic emissions were carried out following guidelines in compliance with ASTM E976/E976M [17].

Table 2. Complete experimental test matrix

Lubricant formulation	Nanoparticle concentration	Quartz concentration	Load	Speed	Test duration	Replicates
Base oil	0 wt%	0.05 wt% (435 mg/L)	1000 N, 2000 N	1000 rpm, 2000 rpm, 3000 rpm	5 h	3
WS_2	0.05 wt%, 0.20 wt%	0.05 wt% (435 mg/L)	1000 N, 2000 N	1000 rpm, 2000 rpm, 3000 rpm	5 h	3
GNP	0.05 wt%, 0.20 wt%	0.05 wt% (435 mg/L)	1000 N, 2000 N	1000 rpm, 2000 rpm, 3000 rpm	5 h	3
Al_2O_3	0.05 wt%, 0.20 wt%	0.05 wt% (435 mg/L)	1000 N, 2000 N	1000 rpm, 2000 rpm, 3000 rpm	5 h	3

All lubricant formulations were evaluated under the same quartz contamination level of 0.05 wt% (435 mg/L) to maintain a controlled contamination severity and enable direct comparison of additive-dependent tribological behavior. Each condition was repeated three times, and the reported values represent the mean response of independent tests.

2.4. Measurement and Data Acquisition

Vibrations were recorded in the radial direction, axial direction and tangential direction using a piezoelectric accelerometer (PCB 352C65, 100 mV.g^{-1}) at a sampling of 50 kHz. A strain-gauge torque transducer (HBM T22, 0.5 N·m) was used to monitor friction torque continuously. Bearing housing temperature is sampled once per second. The calculation of RMS, kurtosis and spectral energy features, derived from signals, is widely employed for bearing diagnosis.

2.5. Surface and Oil Analysis

After every test, the bearings were dismantled and washed in petroleum ether. Surface morphology and wear debris were categorized by scanning electron microscopy (SEM, JEOL JSM-7610F) with Energy-Dispersive Spectroscopy (EDS). The tribochemical composition of the formed films was analyzed using X-ray photoelectron spectroscopy (XPS, Thermo K-Alpha) and Raman spectroscopy (Renishaw inVia Reflex, 532 nm laser). Surface roughness (Ra) before and after testing was measured using a contact profilometer (Mitutoyo SJ-410), and lubricant cleanliness was evaluated by a laser particle counter (Pamas SBSS) following ISO 4406. Elemental analysis of the used oil was carried out via ICP-OES to detect wear metal concentration [18].

2.6. Data Reduction and Statistical Analysis

Tests under each operating condition were performed three times, and mean values with standard deviation error bars were reported [19]. The coefficient of friction (μ) was derived from torque (T) using Equation (1).

$$\mu = \frac{T}{F_n r_m} \quad (1)$$

where, F_n is the applied radial load and r_m is the mean bearing radius.

The specific wear rate was calculated from the measured mass loss using:

$$k = \frac{\Delta V}{F_n S} = \frac{\Delta m}{\rho F_n S} \quad (2)$$

where k is the specific wear rate ($mm^3\ N^{-1}\ m^{-1}$), ΔV is the wear volume (mm^3), Δm is the measured mass loss (g), ρ is the density of the bearing material (gmm^{-3}), F_n is the applied radial load (N), and S is the total running distance (m).

The total running distance was calculated as:

$$S = 2\pi r_m N \quad (3)$$

Where, r_m is the mean bearing raceway radius (m), and N is the total number of shaft revolutions during the test. When the rotational speed is expressed as $n\left(\text{revmin}^{-1}\right)$ and the test duration is $t(\text{ min})$, the total number of revolutions is: $N = nt$.

Before and after each test, the bearing components were cleaned using the same procedure, dried to constant mass, and weighed using an analytical balance with a resolution of 0.1 mg. The reported wear rate represents the mean value obtained from three independent tests.

Each experimental condition was tested independently three times, and the results are reported as mean ± standard deviation. For comparisons among the four lubricant formulations at a fixed load, speed, nanoparticle concentration, and quartz concentration, one-way analysis of variance (ANOVA) was applied, followed by Tukey's Honestly Significant Difference (HSD) test for pairwise comparisons.

For the speed-dependent analysis, two-way ANOVA was applied with lubricant formulation and rotational speed as fixed factors.

Statistical significance was considered at $p < 0.05$. The statistical analysis was performed using OriginPro 2024 (OriginLab Corporation, Northampton, MA, USA).

3. Results and Discussion

3.1. Frictional Behavior and Temperature Trends

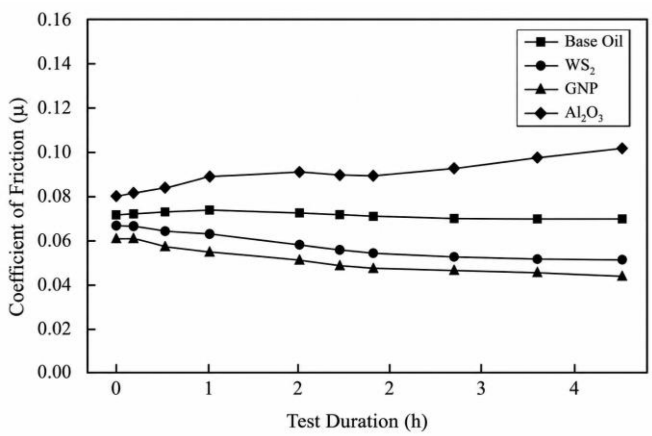

Fig. 2 Changes in the coefficient of friction (μ) over the test duration (h) for base oil, WS_2, GNP, and Al_2O_3-based nano lubricants in the presence of quartz particle contamination (load: 1000 N; speed: 2000 rpm)

Figure 2 shows the change in friction coefficient with time for different lubricants with contaminant containing different nanoparticle additives. For the base oil without additives, the friction coefficient was stable for the initial stage of the test but increased substantially after 2 h or so. This increase is due to the abrasiveness of quartz particles trapped at the contact interface. Throughout the test, the protective surface layer worsened, which increased colliding metal parts and led to a rise in temperature. As a result, there was higher surface asperity interaction leading to higher friction, which aligns with what has already been observed in literature. The Y-axis of Figure 2 represents the value of the coefficient of friction (μ), and on the X-axis total test duration in hours. The temporal evolution of friction under contaminated rolling-contact conditions is shown in Figure 2. [20]. WS_2 and Graphene Nanoplatelets (GNP) helped significantly stabilize the frictional response.

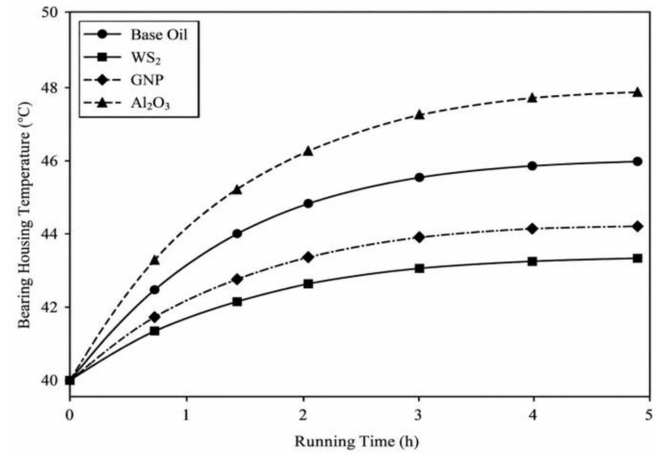

Fig. 3 Variation of bearing housing temperature with running time for different lubricant formulations

Moreover, the WS_2-based lubricant showed the minimum average value of the coefficient of friction (μ=0.065) due to the presence of a low shear tribofilm of WS_2 platelets aligned parallel with the sliding directions. Likewise, the GNP-based lubricant achieved a comparable reduction in friction (μ=0.07), which was due to the formation of a carbonaceous transfer layer, which ultimately lowered the metal-to-metal contact. Conversely, the Al_2O_3 additive extremely generates larger tribological levels (μ=0.09 to 0.1), and the friction curve collectively showed irregular oscillations due to rugged particles agglomeration and interaction with quartz debris. The presence of these particles, which acted as third bodies, increased abrasion while destabilizing EHL film [21]. The temperature development outlined in Figure 3 corresponds well with the friction evolution in this case.

3.2. Effect of Rotational Speed

Table 3. Effect of rotational speed on the measured bearing responses ***(Mean ± standard deviation, Load = 1000 N, Quartz concentration = 0.05 wt%)***

Speed (rpm)	Lubricant formulation	Mean coefficient of friction (μ)	Final temperature (°C)	Vibration RMS (mm/s)	Specific wear rate ($\times10^{-7}$ mm³ N⁻¹ m⁻¹)
1000	Base oil	0.071 ± 0.003	42.1 ± 0.8	1.21 ± 0.09	2.55 ± 0.18
1000	WS_2 (0.05 wt%)	0.061 ± 0.002	39.4 ± 0.6	0.82 ± 0.05	1.02 ± 0.08
1000	GNP (0.05 wt%)	0.065 ± 0.003	40.0 ± 0.7	0.88 ± 0.06	1.25 ± 0.09
1000	Al_2O_3 (0.05 wt%)	0.086 ± 0.004	44.8 ± 0.9	1.65 ± 0.12	2.65 ± 0.20
2000	Base oil	0.078 ± 0.004	46.5 ± 1.0	1.62 ± 0.11	3.05 ± 0.22
2000	WS_2 (0.05 wt%)	0.065 ± 0.002	42.7 ± 0.7	0.98 ± 0.07	1.19 ± 0.10
2000	GNP (0.05 wt%)	0.070 ± 0.003	43.4 ± 0.8	1.04 ± 0.08	1.50 ± 0.11
2000	Al_2O_3 (0.05 wt%)	0.095 ± 0.005	48.9 ± 1.1	2.05 ± 0.15	2.90 ± 0.24
3000	Base oil	0.084 ± 0.005	51.8 ± 1.2	2.08 ± 0.14	3.65 ± 0.28
3000	WS_2 (0.05 wt%)	0.069 ± 0.003	46.1 ± 0.9	1.22 ± 0.09	1.38 ± 0.12
3000	GNP (0.05 wt%)	0.074 ± 0.004	46.9 ± 1.0	1.31 ± 0.10	1.72 ± 0.13
3000	Al_2O_3 (0.05 wt%)	0.102 ± 0.006	54.5 ± 1.3	2.55 ± 0.18	3.45 ± 0.27

The increase in rotational speed from 1000 to 3000 rpm resulted in a gradual increase in friction, temperature, vibration amplitude, and specific wear rate for all lubricant formulations. The increase was more pronounced for the contaminated base oil and Al_2O_3-containing lubricant due to intensified quartz particle entrainment and third-body abrasion. In contrast, WS_2 and GNP maintained lower friction and wear because of the formation of protective tribofilms that reduced direct contact between the bearing surfaces and contaminant particles.

Table 3 compares the tribological and dynamic responses obtained at 1000, 2000, and 3000 rpm. At 3000 rpm, the mean coefficients of friction were 0.084, 0.069, 0.074, and 0.102 for the base oil, WS_2, GNP, and Al_2O_3 formulations, respectively. The corresponding final housing temperatures were 51.8 °C, 46.1 °C, 46.9 °C, and 54.5 °C, while the vibration RMS values were 2.08, 1.22, 1.31, and 2.55 mm/s, respectively.

Compared with the 2000 rpm condition, operation at 3000 rpm increased the coefficient of friction by approximately 7.7% for base oil, 6.2% for WS_2, 5.7% for GNP, and 7.4% for Al_2O_3. The final housing temperature increased by 11.4%, 8.0%, 8.1%, and 11.5%, respectively, whereas vibration RMS increased by 28.4%, 24.5%, 26.0%, and 24.4%. The specific wear rate increased by approximately 19.7%, 16.0%, 14.7%, and 19.0% for base oil, WS_2, GNP, and Al_2O_3, respectively.

The higher rotational speed produced increased frictional heating, vibration response, and wear progression, which can be associated with increased shear losses, reduced lubricant-film stability, enhanced contaminant entrainment, and more frequent quartz particle passage through the rolling contact. WS_2 and GNP retained their protective behaviour at higher speed because of the formation of low-shear tribofilms and carbonaceous transfer layers, whereas Al_2O_3 showed increased abrasive behaviour due to hard-particle interaction and third-body effects.

The formulation effect at 3000 rpm was statistically significant for coefficient of friction ($p = 0.002$), final temperature ($p = 0.004$), vibration RMS ($p = 0.001$), and specific wear rate ($p = 0.003$).

3.3. Vibration and Wear Characteristics

To understand the vibration and wear characteristics completely, the vibration analysis offers a dynamic indication of the tribological condition inside the bearing. Representative samples of time-domain vibration amplitude are shown in Figure 4.

In this case, the contaminated base oil demonstrated a pronounced increase in vibration RMS values after 3 hours of operation, corresponding to the onset of surface degradation. In contrast, with the incorporation of WS_2 and GNP nanoparticles, the vibration amplitude remained comparatively steady throughout the test duration, suggesting improved lubricant film stability. These results are consistent with the protective mechanisms proposed in earlier works. Moreover, the lamellar WS_2 particles filled micro-surface valleys, while the graphene nanoplatelets formed compact transfer layers, both effectively isolating the rolling elements from abrasive contaminants.

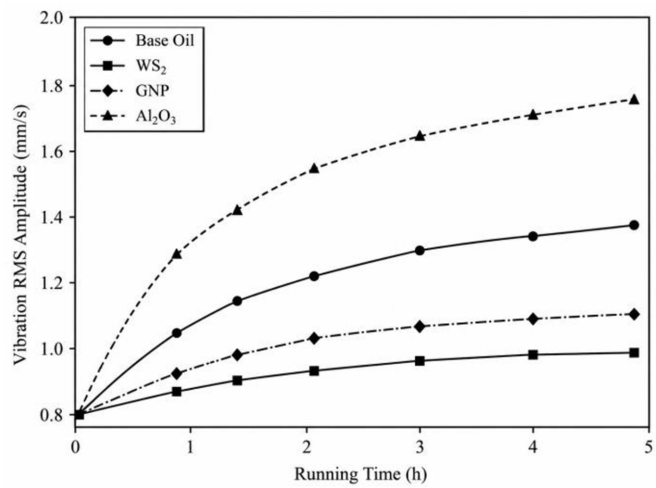

Fig. 4 Time-domain vibration RMS response of bearings lubricated with different nano-additive oils under quartz contamination

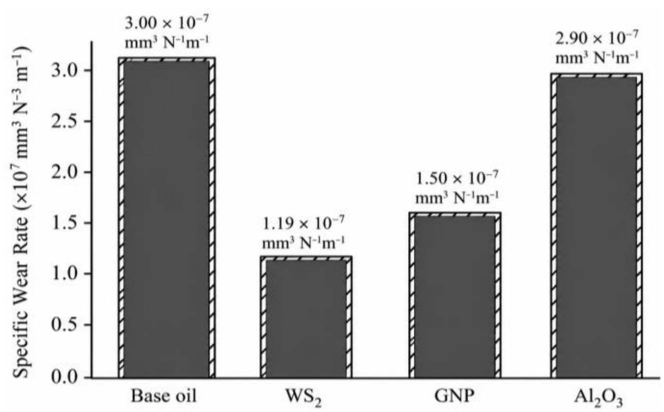

Fig. 5 Comparative wear rate of bearings under various lubricant formulations

In contrast, the lubricant, containing Al2O3, demonstrated intermittent high-frequency spikes and larger kurtosis values, indicating periodic particle impacts. This behaviour supports the view that hard Al_2O_3 nanoparticles, when joined with silica contaminants, endorse abrasive third-body motion. Correspondingly, the specific wear rate (calculated from mass loss and contact conditions) for each lubricant is shown in Figure 5. The WS_2 additive produced the lowest wear rate (1.19×10^{-7} mm³ N⁻¹ m⁻¹), followed by GNP (1.5×10^{-7} mm^3 N^{-1} m^{-1}). On the contrary, the wear rate for the Al_2O_3 sample was nearly double that (2.9×10^{-7} mm^3 N^{-1} m^{-1}), confirming that it was more abrasive. In addition, these results agree with the microstructural observations [23].

3.4. Surface Morphology and Tribofilm Characterization

The analysis of the bearing raceways using SEM carried out post-test Figure 6 (a)-(d), demonstrated distinctive and high-information surface morphologies influenced by each nano-additive. On the contrary, the control sample (base oil without additives) shows clear ploughing grooves and also micro-cutting scars and debris-induced micro-pits, which indicate an active three-body abrasive wear mechanism due to quartz particle ingress. The presence of these deep grooves indicates that hard contaminants may have become trapped and rolled between the rolling element and the mating raceway on numerous occasions. On the other hand, the surface treated with WS_2, in contrast, gave smoother wear tracks with shallow grooves and patch-like regions. These are attributed to the formation of a tribo-chemically derived lamellar WS_2 film. Such tribofilms act as robust lubricating layers. Thus, they accommodate shear and prevent direct asperity interaction.

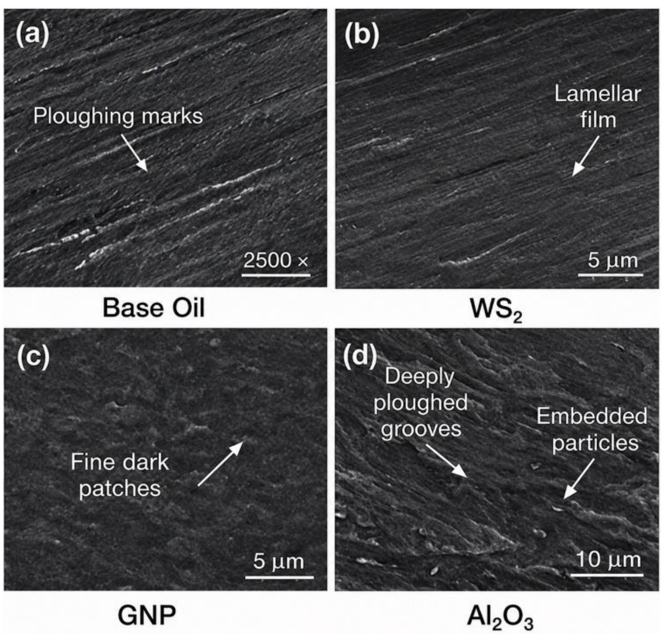

Fig. 6 SEM micrographs of bearing raceways lubricated with, (a) base oil, (b) WS_2, (c) GNP, and (d) Al_2O_3 additives under quartz contamination (Load: 2000 N, Speed: 2000 rpm)

Consequently, they reduce the severity of abrasives. Also, GNP-based lubrication exhibited mixed morphology consisting of small dark patches indicating a graphitic transfer layer and mild grooves. The carbonaceous films help in easy shear and surface passivation, which explains the less wear. In contrast, the lubricant containing Al_2O_3 caused more severe ploughing and embedded particle fragments, which was an enhanced abrasive regime as a result of the synergistic effect between the alumina nanoparticles and quartz contaminant. The presence of tungsten and sulfur peaks confirmed the WS_2-derived tribofilm formation during EDS analysis. The dark patches of the GNP sample were fine and uniformly dispersed, which appear to be graphitic tribofilms, which are solid lubricants and increase surface protection. In contrast, the lubricant based on Al_2O_3 formed irregular grooves and deep grooves, while embedded particles were observed in the rolling path, indicating the abrasive nature of oxide nanoparticles. All in all, these observations are in accordance with the wear data and friction, which have been discussed earlier [24].

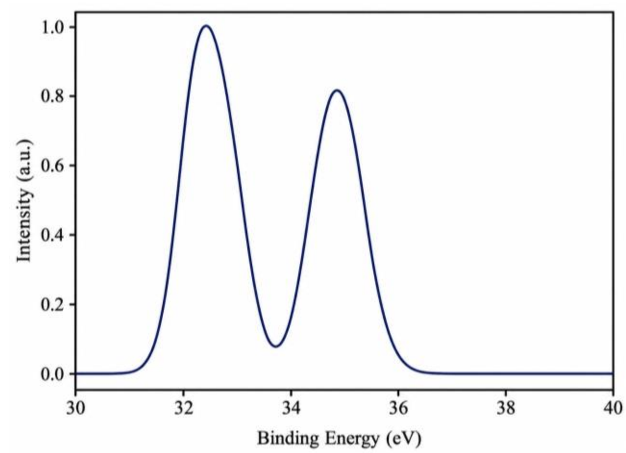

(a)

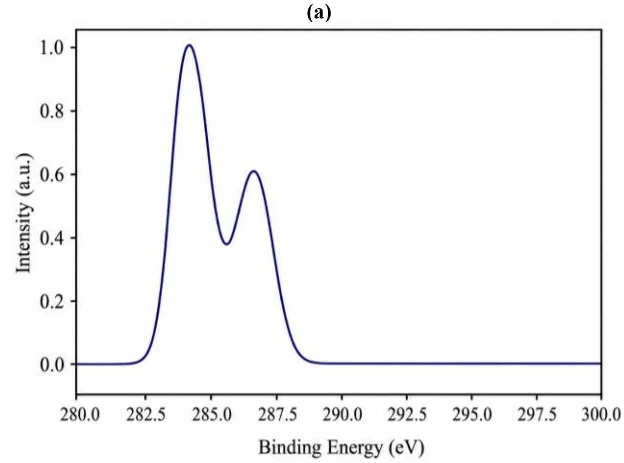

(b)

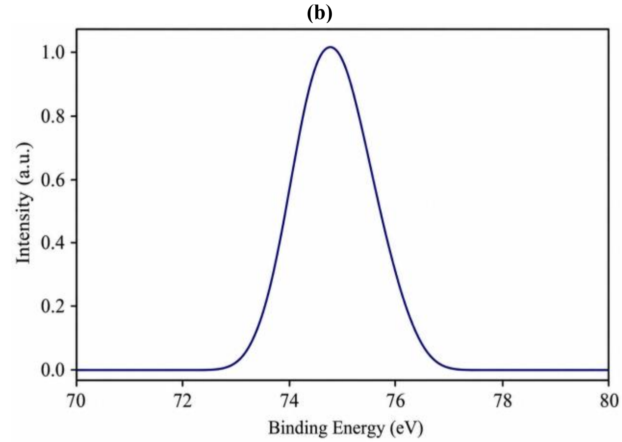

(c)

Fig. 7 XPS spectra of bearing raceway surfaces lubricated with (a) WS_2, (b) GNP, and (c) Al_2O_3 nano-additive formulations under quartz contamination, showing characteristic binding energy peaks corresponding to tribofilm formation and surface interactions

XPS analysis of the tribologically tested surfaces (Figure 7) provided clear evidence of additive-derived tribo-chemical film formation and the associated protective mechanisms. The WS_2-lubricated samples exhibited characteristic W4f doublets, with the W4f$_{7/2}$ and W4f$_{5/2}$ peaks located at approximately 32.6 eV and 34.8 eV, respectively, confirming the presence of tungsten sulfide species on the worn raceway surface. Minor contributions from W–O bonds at higher binding energies indicated mild oxidative transformation during sliding, a behaviour commonly observed for transition-metal dichalcogenides under boundary lubrication. The presence of these lamellar WS_2 compounds suggests that the additive undergoes shear-assisted exfoliation, forming a low-shear-strength tribofilm that separates the surfaces and inhibits abrasive ploughing. The GNP-treated surfaces showed dominant C1s peaks at approximately 284.6 eV (C–C sp^2) and 286.0 eV (C–O), confirming the presence of graphitic carbon on the worn surface. The sp^2-rich carbon network enhances surface passivation and promotes easy shear, thereby reducing mechanical interaction with quartz particles. Conversely, the Al_2O_3-lubricated specimens produced weak tribochemical signatures indicating poor film-forming behaviour. However, peaks related to surface oxides and fragmental debris indicated an abrasive wear mechanism and not tribofilm formation. In addition, the binding energy values were found to have very close agreement with reference values for WS_2, graphene-derived carbon, and Al_2O_3, confirming the chemical nature of the tribofilms formed in operation [25, 26].

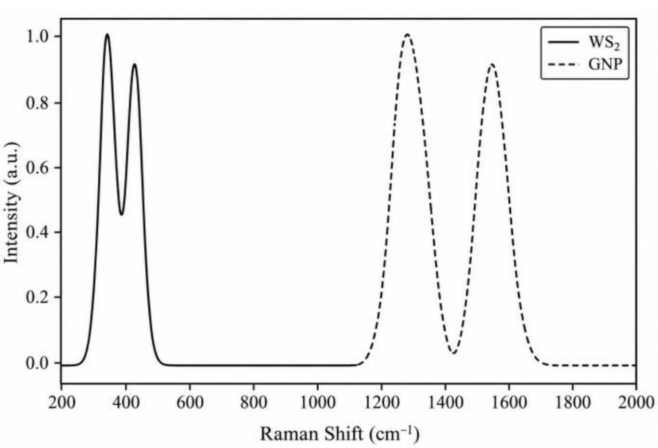

Fig. 8 Raman spectra confirming tribofilm formation on WS_2 and GNP-treated samples

Figure 8 indicates the presence of lubricious WS_2 and graphitic phases on the bearing surfaces, thus confirming previous reports. The presence of crystalline or semi-crystalline WS_2 lamellae on the bearing track is confirmed by the observation of vibrational modes at 350 cm^{-1} (E_2g^1) and 420 cm^{-1} (A_1g) of the WS_2-lubricated specimens. [27] The shear-induced exfoliation and partial disordering of these peaks due to sliding are the main reasons for the moderate broadening as seen in layered solid lubricants at relatively high contact stresses. Graphitic tribofilm deposition was indicated on the GNP-treated surfaces by the presence of the D (1350-1460 cm^{-1}) and G (1580-1600 cm^{-1}) bands. According to the D/G intensity ratio, the carbon layer possesses a moderate level of disorder. This agrees with the sliding-induced fragmentation as well as the re-organization of graphene sheets.

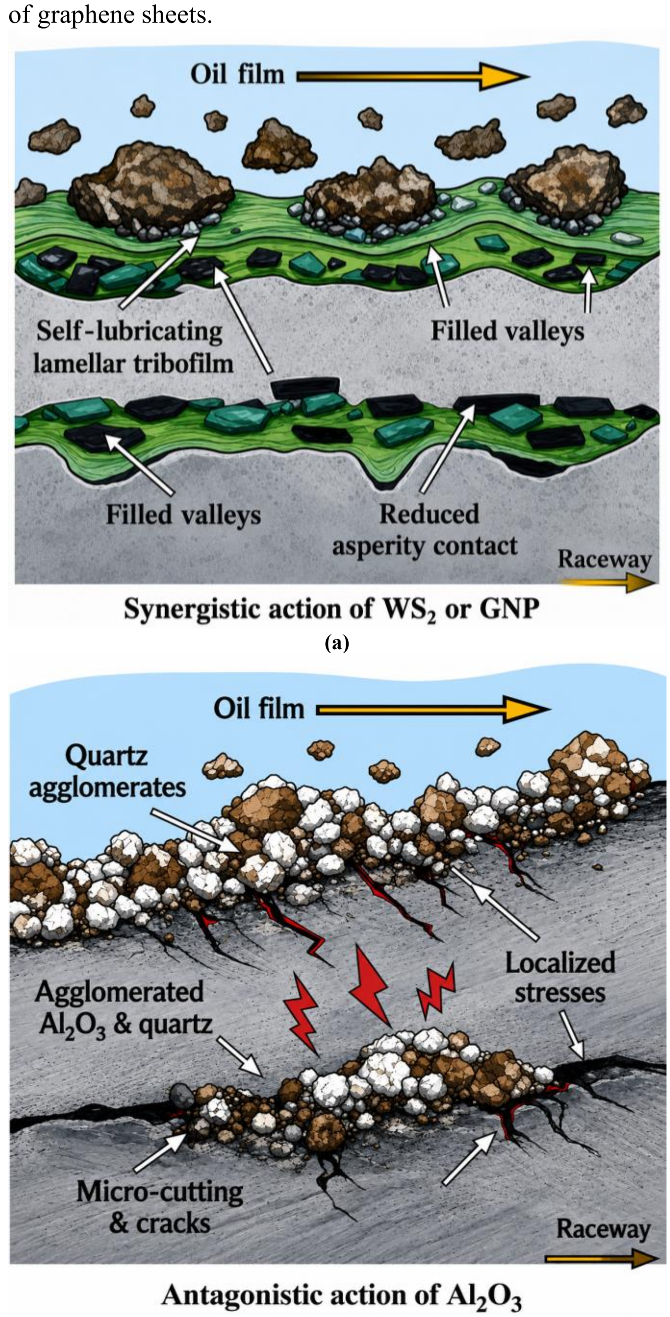

(a)

(b)

Fig. 9 Schematic illustration of (a) synergistic (WS_2, GNP) and (b) antagonistic (Al_2O_3) mechanisms of nanoparticle–contaminant interaction in lubricated contacts

Disordered graphitic films are reported to enable ease of sliding and friction reduction. On the contrary, the Al_2O_3-based lubrication Raman spectra exhibited a lack of identifiable additive signatures. The absence of stable tribochemical species backs up the abrasive wear mechanism of SEM [28]. Based on the wear-rate values shown in Figure 5, WS_2 and GNP reduced specific wear by approximately 60.3% and 50.0%, respectively, relative to the contaminated base oil. In contrast, Al_2O_3 produced only a small change in wear rate and retained extensive abrasive surface damage. The superior response of WS_2 is attributed to the formation of a low-shear tungsten–sulfur-rich layer that accommodates interfacial shear and limits direct quartz–steel interaction. GNP provides protection through a carbon-rich transfer layer, although its performance depends on the continuity and retention of the deposited film. Al_2O_3 does not provide the same low-shear mechanism. Its high hardness and agglomeration with quartz increase local contact stress, particle indentation, and micro-cutting. Earlier investigations have commonly examined either nano-additives in relatively clean lubricants or contaminant-induced bearing damage without detailed tribofilm chemistry. The present study extends those findings by linking friction, temperature, vibration, wear, morphology, and surface chemistry under the same contaminated rolling-contact condition. Because test rigs, loads, speeds, oils, particle concentrations, and wear calculations differ among studies, direct claims of numerical superiority should be avoided. The contribution should instead be presented as a broader mechanistic comparison under controlled contamination.

3.5. Mechanism of Additive–Contaminant Interaction

Figure 9 displays a mechanistic model for the interaction of the additive and contaminant, based on the tribological, vibrational and chemical analysis. The roles of WS_2 and GNP nanoparticles were synergistic with the contaminant through filling the microvalleys, forming self-lubricating tribofilms and reducing the asperity contact. In contrast, particles of Al_2O_3 showed an adverse effect as they agglomerated with silica impurities and enhanced localized stresses, which led to micro-cutting and fatigue cracks. In accordance with the indications, it can be affirmed that the nanoparticles produce varying results depending on their hardness, morphology, and surface reactivity. The WS_2 and GNP formulations thus exhibit much superior resistance to frictional heating and wear, which shows their practical potential in designing contaminant-tolerant lubricants for industrial bearings [29, 30].

4. Conclusion

This study shows that the performance of a nano-additive under clean lubrication cannot automatically be extended to a particle-contaminated rolling contact. Under quartz contamination, WS_2 and GNP retained protective behaviour through the formation of low-shear additive-derived surface films. In contrast, Al_2O_3 intensified third-body abrasion because the hard oxide particles interacted and agglomerated with quartz debris. The main contribution of the study is the side-by-side mechanistic comparison of lamellar WS_2, sheet-like GNP, and hard ceramic Al_2O_3 under the same contaminated bearing conditions. The combined friction, temperature, vibration, wear, SEM/EDS, XPS, and Raman results connect the measured bearing response with the formation or absence of a protective tribofilm. At the reference operating condition, WS_2 produced the lowest specific wear rate of 1.19×10^{-7} mm³ N⁻¹ m⁻¹, followed by GNP at 1.50×10^{-7} $mm^3\ N^{-1}\ m^{-1}$. From an engineering perspective, the findings support the use of film-forming WS_2 and GNP additives in bearings exposed to particulate ingress. They also show that the addition of a nanoparticle is not necessarily beneficial, particularly when the additive hardness and agglomeration behaviour increase abrasive third-body interactions.The study is limited to one bearing type, one base oil, one quartz-particle size range, laboratory contamination, and relatively short test durations. The long-term stability of the nanoparticle dispersions and their effects on rolling-contact fatigue life were not examined. Future investigations should consider longer operating periods, wider contaminant concentrations and particle-size distributions, aged lubricants, dispersion-stability measurements, repeated start–stop cycles, and validation in full-scale industrial machinery.

Conflicts of Interest

The authors declare that they have no conflicts of interest.

Funding Statement

This research received no external funding.

Acknowledgments

The authors acknowledge the support received during the course of this research.

References

[1] Paul C. Uzoma et al., “Tribology of 2D Nanomaterials: A Review,” *Coatings*, vol. 10, no. 9, pp. 1-27, 2020. [CrossRef] [Google Scholar] [Publisher Link]

[2] Aidil Ikhsan, Dedison Gasni, and Meifal Rusli, “Wear Patterns on Ball Bearings Lubricated by Grease Contaminated with Several Large Solid Particles,” *Tribology in Industry*, vol. 47, no. 2, pp. 202-216, 2025. [CrossRef] [Google Scholar] [Publisher Link]

[3] Ewa Piątkowska, “Influence of Solid Particle Contamination on the Wear Process in Water-Lubricated Marine Strut Bearings with NBR and PTFE Bushes,” *Polish Maritime Research*, vol. 28, no. 4, pp. 167-178, 2021. [CrossRef] [Google Scholar] [Publisher Link]

[4] Michael Maier, Michael Pusterhofer, and Florian Grün, “Wear Simulation in Lubricated Contacts Considering Wear-Dependent Surface Topography Changes,” *Materials Today: Proceedings*, vol. 93, pp. 563-570, 2023. [CrossRef] [Google Scholar] [Publisher Link]

[5] Yonggang Meng et al., “A Review of Recent Advances in Tribology,” *Friction*, vol. 8, no. 2, pp. 221-300, 2020. [CrossRef] [Google Scholar] [Publisher Link]

[6] Yonggang Meng et al., "A Review of Advances in Tribology in 2020–2021," *Friction*, vol. 10, no. 6, pp. 1443-1595, 2022. [CrossRef] [Google Scholar] [Publisher Link]

[7] Amrut S. Aher, and Vijay Kumar Pandey, "Insight on the Effect of Nanoparticles Addition in Oil Lubrication: A Review," *Tribology in Industry*, vol. 45, no. 3, pp. 444-456, 2023. [CrossRef] [Google Scholar] [Publisher Link]

[8] Muhammad Waqas et al., "A Review of Friction Performance of Lubricants with Nano Additives," *Materials*, vol. 14, no. 21, pp. 1-24, 2021. [CrossRef] [Google Scholar] [Publisher Link]

[9] Zhengquan Jiang et al., "Research Progresses of Nanomaterials as Lubricant Additives," *Friction*, vol. 12, no. 7, pp. 1347-1391, 2024. [CrossRef] [Google Scholar] [Publisher Link]

[10] Zhengquan Jiang et al., "Synthesis of Oil-Soluble WS2 Nanosheets under Mild Condition and Study of Their Effect on Tribological Properties of Poly-Alpha Olefin under Evaluated Temperatures," *Tribology International*, vol. 138, pp. 68-78, 2019. [CrossRef] [Google Scholar] [Publisher Link]

[11] Jia Ren et al., "Investigation of the Tribological Performances of Graphene and WS2 Nanosheets as Additives for Perfluoroalkylpolyethers Under Simulated Space Environment," *Tribology Letters*, vol. 69, no. 2, pp. 1-13, 2021. [CrossRef] [Google Scholar] [Publisher Link]

[12] Xiufang Bai et al., "Tribological Performance of Different Concentrations of Al2O3 Nanofluids on Minimum Quantity Lubrication Milling," *Chinese Journal of Mechanical Engineering*, vol. 36, no. 1, pp. 1-12, 2023. [CrossRef] [Google Scholar] [Publisher Link]

[13] Jyoti Srivastava, Tandra Nandi, and Rakesh Kumar Trivedi, "Experimental Investigations on Thermophysical, Tribological and Rheological Properties of MoS2 and WS2 Based Nanolubricants with Castor Oil as Base Lubricant," *Tribology in Industry*, vol. 45, no. 4, pp. 591-603, 2023. [CrossRef] [Google Scholar] [Publisher Link]

[14] Filip Ilie, and Andreea-Catalina Cristescu, "A Study on the Tribological Behavior of Molybdenum Disulfide Particles as Additives," *Coatings*, vol. 12, no. 9, pp. 1-10, 2022. [CrossRef] [Google Scholar] [Publisher Link]

[15] Johny Tannous et al., "Understanding the Tribochemical Mechanisms of IF-MoS2 Nanoparticles Under Boundary Lubrication," *Tribology Letters*, vol. 41, no. 1, pp. 55-64, 2011. [CrossRef] [Google Scholar] [Publisher Link]

[16] Zahrul Fuadi et al., "Effect of Graphene Nanoplatelets on Tribological Properties of Bacterial Cellulose/Polyolester Oil Bio-Lubricant," *Frontiers in Mechanical Engineering*, vol. 8, pp. 1-11, 2022. [CrossRef] [Google Scholar] [Publisher Link]

[17] Niveditha Noble et al., "Effect of Nano-Additives on Tribological Behaviour of Hazelnut Oil and Sunflower Oil," *Tribology in Industry*, vol. 45, no. 3, pp. 457-471, 2023. [CrossRef] [Google Scholar] [Publisher Link]

[18] Mohamed Kamal Ahmed Ali, Hou Xianjun, and Hua Jiang, "Lubrication Mechanism Analysis of Nickel-Carbon-Based Tribological Layer on Sliding Interfaces in Automotive Engines," *Tribology International*, vol. 195, 2024. [CrossRef] [Google Scholar] [Publisher Link]

[19] Vicente Cortes et al., "The Performance of SiO2 and TiO2 Nanoparticles as Lubricant Additives in Sunflower Oil," *Lubricants*, vol. 8, no. 1, pp. 1-13, 2020. [CrossRef] [Google Scholar] [Publisher Link]

[20] Poppy Puspitasari et al., "Tribology Characteristic of Ball Bearing SKF RB-12.7/G20W using SAE 5W-30 Lubricant with Carbon-Based Nanomaterial Addition," *Tribology in Industry*, vol. 45, no. 4, pp. 664-675, 2023. [CrossRef] [Google Scholar] [Publisher Link]

[21] Jinqiang Shao et al., "Recent Advances in Biomimetic Related Lubrication," *Lubricants*, vol. 12, no. 11, pp. 1-39, 2024. [CrossRef] [Google Scholar] [Publisher Link]

[22] Hong Zhang et al., "Tribological Behavior of WS2 Nanoparticles as Additives in Calcium Sulfonate Complex–Polyurea Grease," *Lubricants*, vol. 11, no. 6, pp. 1-14, 2023. [CrossRef] [Google Scholar] [Publisher Link]

[23] Ajoy Sahu, and Niharendu Saha, "Comparative Investigation of Lubricant Properties of Pongamia and Castor Oil Bio Lubricant Blended with (SAE20W40) Mineral Oil," *Tribology in Industry*, vol. 46, no. 3, pp. 535-547, 2024. [CrossRef] [Google Scholar] [Publisher Link]

[24] Ravikiran et al., "Experimental Study on Tribological, Rheological and Bio-Degradability Characteristics of Canola Oil with TiO2 Nanoparticles as Bio-Nanolubricants," *Tribology in Industry*, vol. 46, no. 3, pp. 458-466, 2024. [CrossRef] [Google Scholar] [Publisher Link]

[25] Xudong Zhao, and Yimin Zhang , "Tribological and Dynamic Performance Analysis of Rolling Bearings with Varied Surface Textures Operating under Lubricant Contamination," *Wear*, vol. 532-533, 2023. [CrossRef] [Google Scholar] [Publisher Link]

[26] Thi-Na Ta et al., "Tribological Characteristics and Vibration Response of Grease Lubricated Contacts under Environmental Particles and Water Impact," *Wear*, vol. 550-551, 2024. [CrossRef] [Google Scholar] [Publisher Link]

[27] Yuyang Yuan et al., "Evaluation of Nanoparticles for Nanoscale Film Fabrication Harnessing Tribochemistry," *Tribology International*, vol. 210, pp. 1-11, 2025. [CrossRef] [Google Scholar] [Publisher Link]

[28] Bharat Kumar et al., "Influence of Nano-Lubrication on Tribological Behavior of AZ91 Magnesium Alloy Under Fretting Condition," *Tribology in Industry*, vol. 45, no. 3, pp. 375-386, 2023. [CrossRef] [Google Scholar] [Publisher Link]

[29] Gaurab Kumar Ghosh et al., "A Multi-Faceted Review on Industrial Grade Nanolubricants: Applications and Rheological Insights with Global Market Forecast," *Results in Engineering*, vol. 25, pp. 1-19, 2025. [CrossRef] [Google Scholar] [Publisher Link]

[30] Bahaa M. Kame et al., "Optimization of the Rheological Properties and Tribological Performance of SAE 5w-30 Base Oil with Added MWCNTs," *Lubricants*, vol. 9, no. 9, pp. 1-13, 2021. [CrossRef] [Google Scholar] [Publisher Link]